Motion Tracking using Nonlinear Gradient Fields: Experimental Verification and Oblique Slices

Kopanoglu E, Wang H, Galiana G, Constable RT
Diagnostic Radiology, Yale University, New Haven, CT, USA.

Synopsis

Motion navigation using nonlinear gradient fields is demonstrated experimentally. The method makes use of the simultaneous multi-dimensional encoding capabilities of nonlinear gradient fields. A two-dimensional navigator image is obtained from a single-echo encoded using a nonlinear gradient field and multiple receiver coils. Without exceeding the maximum field generated by the linear gradient fields of a 3T scanner inside a 20cm isotropic field-of-view, the navigator can be acquired in under one millisecond, including its rewinder. The method can track both translational and rotational in-plane rigid body motion, as demonstrated in phantom experiments. Simulations show the method is applicable in oblique angles.

Purpose

With several MRI applications lasting several minutes, MRI is prone to patient motion. In-slice motion can be corrected in post-processing when motion is tracked. Orbital [1-3], pencil-beam[4-6], spherical [7] and volumetric [8] motion navigators use additional gradient waveforms every TR or separate interleaved TRs whereas marker-based methods, MRI-based [9] or optical [10-12], use markers placed on the body of interest for motion tracking. Marker-based techniques may suffer from false positives due to facial expressions, while motion navigators affect the sequence timing substantially due to the additional waveforms/TRs. Arguably the most commonly used technique is the PROPELLER, which acquires data in an overlapping manner and estimates motion from the overlapping data. Nevertheless, the overlapping acquisition increases the scan time by ~57%, compared to a non-overlapping approach [13,14]. Other techniques keep sequence timing unaltered [15,16] but cannot track rotational motion. Last year, we introduced a motion navigator that uses nonlinear gradient fields to encode translational and rotational motion [17]. The technique uses the simultaneous multi-dimensional encoding capabilities of NLGFs to encode motion using a single echo and with a time-penalty of less than a millisecond. In this abstract, we demonstrate the technique experimentally for rotational and translational motion.

Methods

Experiments were performed using a 3T scanner with an 8-channel receiver-array [Siemens Healthcare, Erlangen, Germany; sensitivities characterized as outlined in [18]] and a Z2-harmonic ($x^2 + y^2 - 2z^2$) gradient insert (Resonance Research Inc, Billerica, MA, USA) controlled using a transmit-array architecture. In the first experiment, translational motion tracking capabilities of the method were tested. A circular cylindrical phantom (Model No: 8624186 K2285, diameter: 12 cm, Siemens Healthcare, Erlangen, Germany) was imaged using a spin-echo sequence and motion encoded at 8 different locations. Spin-echo parameters were; resolution, 128x128; flip-angle, 90-degrees; echo-time, 11ms; repetition-time, 500ms. Motion navigator parameters were NLGF amplitude, 30mT/m^2; readout duration, 6.25 ms; readout samples, 256. In the second experiment, a custom-phantom with a rounded rectangular cross-section was imaged at 8 locations and orientations for tracking both rotational and translational motion. By randomly selecting k-space lines and corresponding motion encoding data from these datasets, composite image k-space and motion datasets were generated separately for each experiment. The maximum rotation angle was determined to be 9.8-degrees. Spin-echo images were obtained using a single-channel coil. All images were

reconstructed to 256x256 resolution. Navigator images were reconstructed using Kaczmarz with 5 iterations and λ=0.02 to prevent the algorithm from converging to erroneous local minima due to the non-unique nature of the spatial encoding matrix (Figure 1) while motion-compensated images were reconstructed using two iterations and $\lambda = 1$ since spatial encoding functions were orthogonal for spin-echo images.

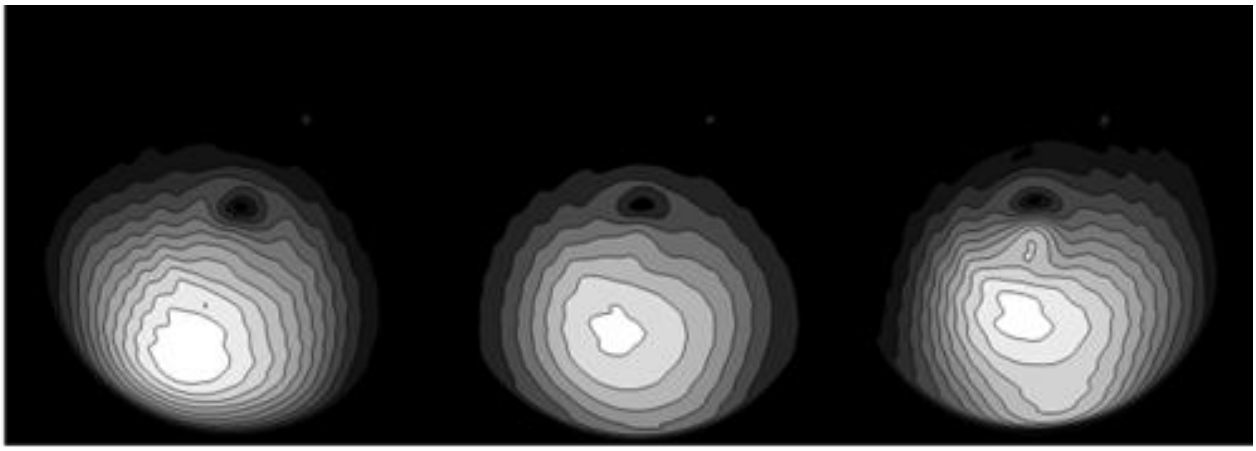

Figure 1: *Motion navigator images reconstructed to a resolution of 256x256 using 6.25ms long single-echo readouts with 256 samples. Data were acquired by imaging a cylindrical phantom at three different locations.*

The NLGF and the disturbance in the static magnetic field were determined using a field mapping sequence [17] and a larger phantom (diameter: 20cm). Spatial and temporal polynomial fitting were performed on the disturbance field and the difference between the two measurements to assess the true nature of the applied NLGF (Figure 2).

Finally, simulations demonstrate the applicability of the method oblique slices.

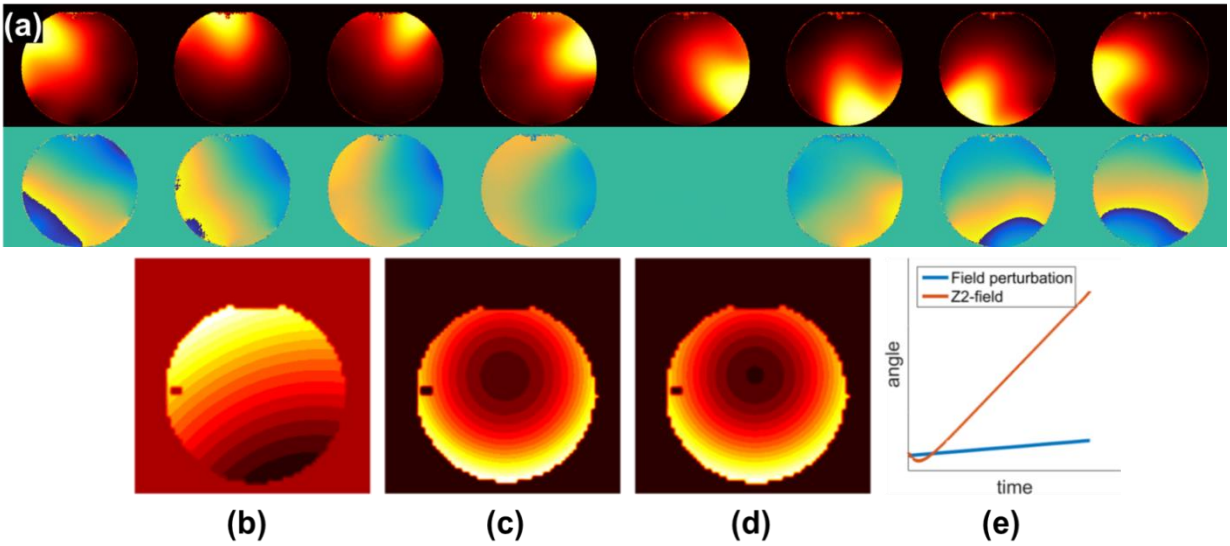

Figure 2: *Experimental RF and gradient fields used in reconstruction. (a) Magnitude and phase images for the RF receiver array. Measured field in absence (b) and presence (c) of the Z2-harmonic field. (d) Second-order spatial fit for the difference between (b) and (c). (e) Temporal fits for (b) and (d).*

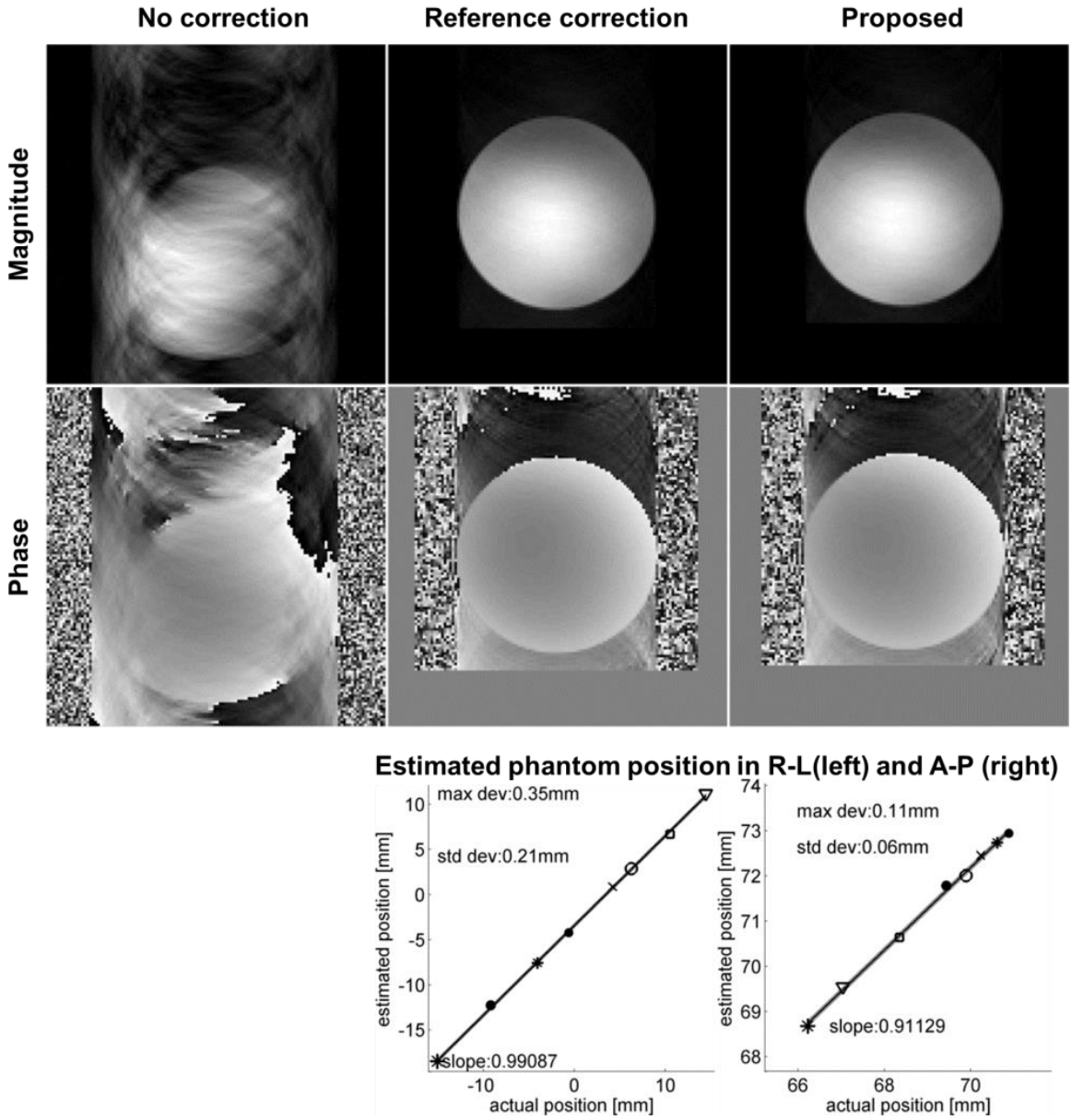

Figure 3: *Translational motion experiment results. Phantom was moved to the center of the FoV after motion correction. Reference images were motion-compensated using location estimation values obtained from spin-echo images. Bottom row displays estimated position information with respect to the actual positions estimated from the full spin-echo datasets.*

Results

For translational motion, the maximum deviation from the actual motion values (determined using images reconstructed from full spin-echo datasets at each location) was less than 0.35 mm in the Right-Left direction and 0.11 mm in Anterior-Posterior, with the standard deviations being 0.21 mm and 0.06 mm, respectively (Figure 3).

For rotational motion, the mean and the standard deviation of the estimation error were -0.07-degrees and 0.23-degrees, respectively (Figure 4).

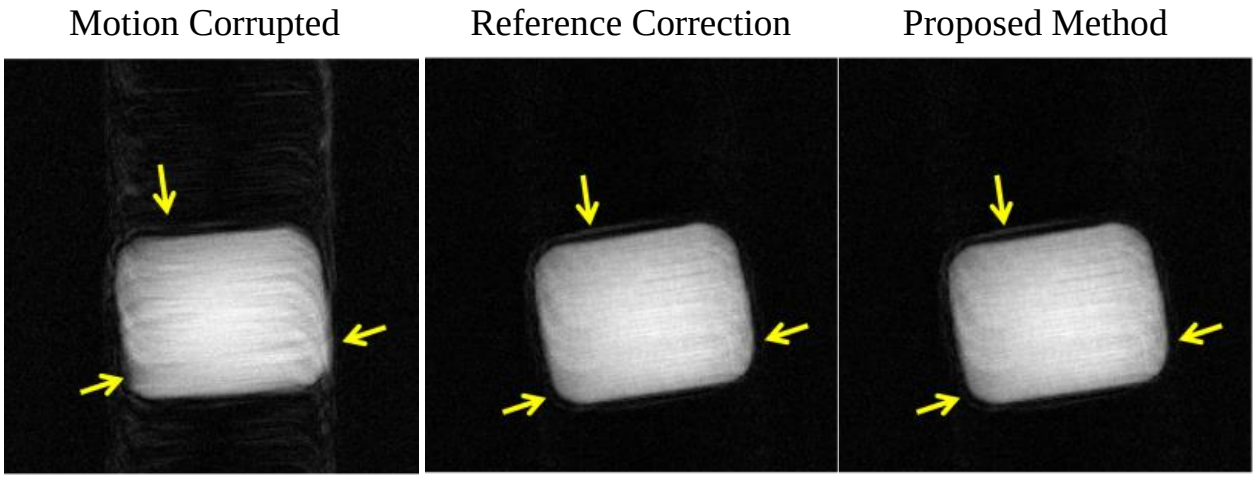

Figure 4: *Rotational motion experiments.* ***Left:*** *motion corrupted images.* ***Right****: the artifacts are reduced and the phantom image is well-recovered after correction. The halo around the phantom is due to the phantom's shape, and is apparent in the reference correction (middle-panel, corrected using motion estimated from spin-echo images) as well.*

Discussion

With the proposed navigation scheme, the outer-most and inner-most edges of the imaged object are determined via frequency encoding while the other edges are determined using parallel imaging [17]. Hence, the method would benefit from a receiver-array with more coils. Nevertheless, phantom locations were selected to be offset in the Posterior direction to test the efficacy of the method when the object is closer to a subset of coils (effective number of coils decreases). Hence, frequency encoding was more effective in the A-P direction, yielding a lower estimation error.

Simulations (Figure5) show that motion tracking can be performed in oblique slices and other field shapes also can be used for 2D navigation using a single-echo as long as the field varies along at least two directions simultaneously.

The maximum field generated inside a $(10cm)^3$ isotropic volume was 0.3mT for navigation. By increasing the NLGF amplitude such that the maximum field generated by the linear gradient fields of the system (40mT/m) inside the same volume is not exceeded, the navigator data can be acquired in less than half a millisecond, reducing the navigator length to less than a millisecond including the rewinder-waveform.

Conclusion

Motion navigation using nonlinear gradient magnetic fields [17] was demonstrated experimentally with sub-pixel and sub-degree accuracy for translational and rotational in-slice rigid body motion.

Acknowledgements

R01-EB012289, R01-EB016978

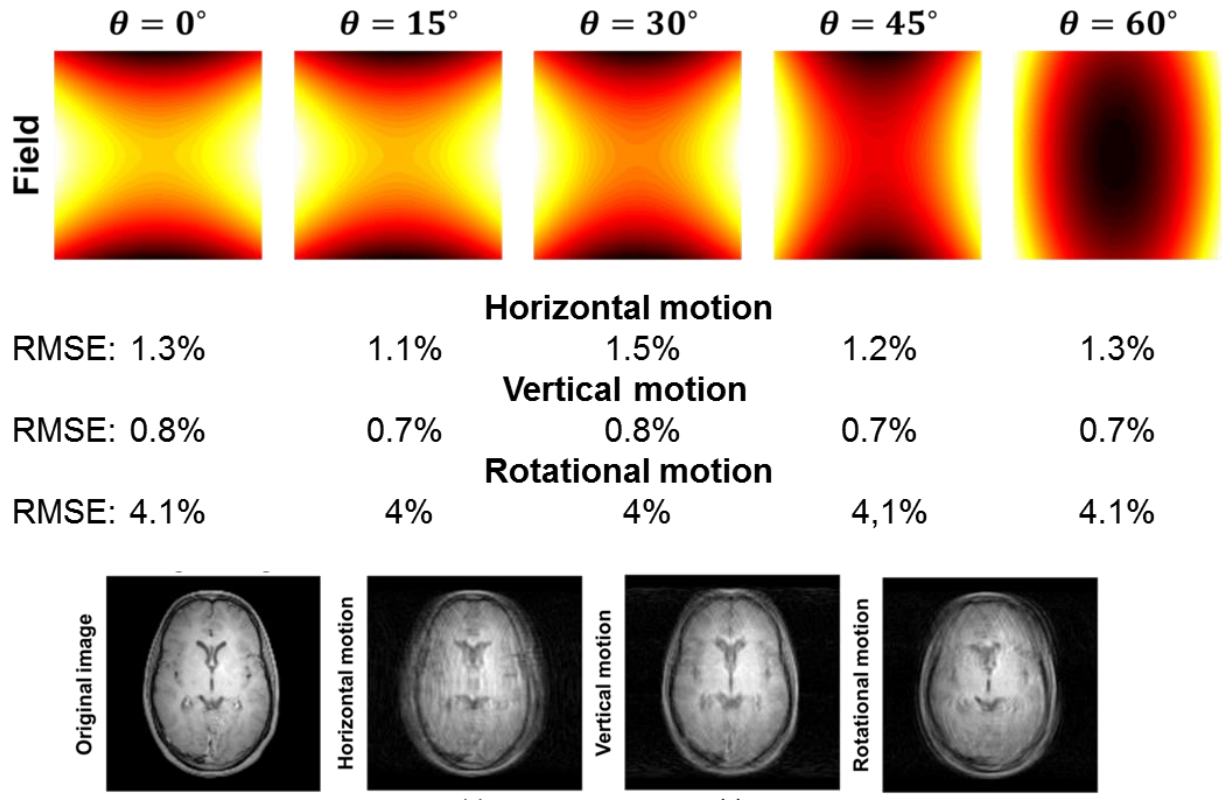

Figure 5: *The method was demonstrated for oblique angles (θ measured from the longitudinal axis). Simulation parameters were same as reported in (17). The coronal slice ($\theta = 0$) suggests the method can be applied using the C2- and S2- harmonics as well.*

REFERENCES

1. Fu ZW, Wang Y, Grimm RC, Rossman PJ, Felmlee JP, Riederer SJ, Ehman RL. Orbital navigator echoes for motion measurements in magnetic resonance imaging. Magnetic Resonance in Medicine 1995;34(5):746-753.
2. Lee CC, Jack CR, Grimm RC, Rossman PJ, Felmlee JP, Ehman RL, Riederer SJ. Real-time adaptive motion correction in functional MRI. Magnetic Resonance in Medicine 1996;36(3):436-444.
3. Lee CC, Grimm RC, Manduca A, Felmlee JP, Ehman RL, Riederer SJ, Jack CR. A prospective approach to correct for inter-image head rotation in FMRI. Magnetic Resonance in Medicine 1998;39(2):234-243.
4. Kozerke S, Schär M, Lamb HJ, Boesiger P. Volume tracking cardiac 31P spectroscopy. Magnetic Resonance in Medicine 2002;48(2):380-384.
5. Köhler MO, Denis de Senneville B, Quesson B, Moonen CTW, Ries M. Spectrally selective pencil-beam navigator for motion compensation of MR-guided high-intensity focused ultrasound therapy of abdominal organs. Magnetic Resonance in Medicine 2011;66(1):102-111.
6. Mette KS, Sjoerd PMC, Bernard AZ, Maurits MB, Marco van V, Jan JWL, Bas WR. Navigators for motion detection during real-time MRI-guided radiotherapy. Physics in Medicine and Biology 2012;57(21):6797.

7. Welch EB, Manduca A, Grimm RC, Ward HA, Jack Jr CR. Spherical navigator echoes for full 3D rigid body motion measurement in MRI. Magnetic Resonance in Medicine 2002;47(1):32-41.
8. Tisdall MD, Hess AT, Reuter M, Meintjes EM, Fischl B, van der Kouwe AJW. Volumetric navigators for prospective motion correction and selective reacquisition in neuroanatomical MRI. Magnetic Resonance in Medicine 2012;68(2):389-399.
9. Ooi MB, Aksoy M, Maclaren J, Watkins RD, Bammer R. Prospective motion correction using inductively coupled wireless RF coils. Magnetic Resonance in Medicine 2013;70(3):639-647.
10. Zaitsev M, Dold C, Sakas G, Hennig J, Speck O. Magnetic resonance imaging of freely moving objects: prospective real-time motion correction using an external optical motion tracking system. NeuroImage 2006;31(3):1038-1050.
11. Forman C, Aksoy M, Hornegger J, Bammer R. Self-encoded marker for optical prospective head motion correction in MRI. Medical Image Analysis 2011;15(5):708-719.
12. Singh A, Zahneisen B, Keating B, Herbst M, Chang L, Zaitsev M, Ernst T. Optical tracking with two markers for robust prospective motion correction for brain imaging. Magn Reson Mater Phy 2015:1-12.
13. Pipe JG. Motion correction with PROPELLER MRI: application to head motion and free-breathing cardiac imaging. Magnetic Resonance in Medicine 1999;42(5):963-969.
14. Pipe JG, Gibbs WN, Li Z, Karis JP, Schar M, Zwart NR. Revised motion estimation algorithm for PROPELLER MRI. Magnetic Resonance in Medicine 2014;72(2):430-437.
15. Lustig M, Cunningham C, Daniyalzade E, Pauly J. Butterfly: a self navigating Cartesian trajectory. 2007. p 194.
16. Bookwalter CA, Griswold MA, Duerk JL. Multiple Overlapping k-Space Junctions for Investigating Translating Objects (MOJITO). Medical Imaging, IEEE Transactions on 2010;29(2):339-349.
17. Kopanoglu E, Galiana G, Constable RT. Motion Navigation using Non-Linear Gradient Fields. 2015; Toronto, Canada. p 3674.
18. Walsh DO, Gmitro AF, Marcellin MW. Adaptive reconstruction of phased array MR imagery. Magnetic Resonance in Medicine 2000;43(5):682-690.